AGU PUBLICATIONS

Journal of Advances in Modeling Earth Systems

RESEARCH ARTICLE
10.1002/2017MS001084

Nonlocality of Tropical Cyclone Activity in Idealized Climate Simulations

T. Frisius[1] and S. M. A. Abdullah[1]

[1]Meteorological Institute, Universität Hamburg, Hamburg, Germany

Key Points:
- Sensitivity of tropical cyclones in the climate system to local SST anomalies
- Simulation of nonlocality within the global atmospheric climate model PlaSim
- Large response of tropical cyclone ACE index due to modification of the large-scale circulation

Correspondence to:
T. Frisius,
Thomas.Frisius@uni-hamburg.de

Citation:
Frisius, T., & Abdullah, S. M. A. (2017). Nonlocality of tropical cyclone activity in idealized climate simulations. *Journal of Advances in Modeling Earth Systems*, *9*, 3099–3115. https://doi.org/10.1002/2017MS001084

Received 12 JUN 2017
Accepted 5 DEC 2017
Accepted article online 13 DEC 2017
Published online 29 DEC 2017

Abstract The response of tropical cyclone activity in the predicted warmer future climate is still a topic of scientific research. However, by the nonlocality hypothesis, tropical cyclone activity depends rather on relative than absolute sea surface temperature (SST). This hypothesis is investigated through idealized experiments performed with the global atmospheric climate model PlaSim. The model includes a prescribed SST and adopts a spectral resolution of T170 for resolving tropical cyclones. An idealized land-sea configuration with two oceans and two continents has been used to study the nonlocality mechanism. The sensitivity experiments WARMBASIN and COLDBASIN include a positive and negative SST anomaly of 2.5 K in the northeastern basin. The tropical cyclone activity in the control run is similar in all four ocean basins while experiment WARMBASIN simulates a striking local increase of tropical cyclones. However, they nearly vanish in the other three ocean basins. The response is weaker and in the opposite way in COLDBASIN with a local reduction and a nonlocal increase. Analysis of well-known cyclogenesis indices shows that nonlocality could be explained by the vorticity, relative humidity, and upper tropospheric temperature changes in experiment WARMBASIN while only vorticity is in agreement with nonlocality in experiment COLDBASIN. The vorticity anomalies determine the presence or absence of a steady state large-scale low at the location where tropical cyclones favorably form. This low is modified by an SST-induced change of a Walker-like planetary circulation.

1. Introduction

The estimation of tropical cyclone activity in future climates is still an issue of current research. Future projections reveal large uncertainties of the change of tropical cyclone frequency due to uncertainties in the projected sea surface temperature (SST) pattern (Zhao & Held, 2012). The most obvious assumption that a global mean increase of sea surface temperature (SST) leads to more and more intense tropical cyclones may turn out as too a narrow perspective. Several studies based on global climate model simulations rather hint at a decrease of tropical cyclone frequency due to global warming (e.g., Bacmeister et al., 2016; Bengtsson et al., 2007; Oouchi et al., 2006; Sugi et al., 2009; Zhao et al., 2009). On the other hand, intense tropical cyclones increase in their frequency in many of these climate projections. Other studies have found that a nonlocality of tropical cyclone activity appears in the climate system and may, therefore, be of importance for the impact of global warming (see Emanuel, 2010b; Knutson et al., 2010b; Swanson, 2008; Vecchi & Soden, 2007; Vecchi et al., 2008; Zhao & Held, 2012). Nonlocality means that tropical cyclone activity depends rather on relative SST (local SST minus tropical mean SST) than on absolute SST. Therefore, a local increase of SST in one ocean basin would lead to a decrease of tropical cyclone activity in all other basins although on average a warming of SST has taken place in the tropics. An explanation for the nonlocality effect may result from the relationship between the region with highest SST and the tropical tropospheric temperature (Sobel et al., 2002). Warming of SST yields more deep convection which in turn warms the whole tropical troposphere by dynamical adjustment. Consequently, the static stability rises in the remote basins with the effect of constraining tropical cyclone formation. A relationship between El Niño Southern Oscillation and the tropical cyclone activity in the Atlantic was explained by Tang and Neelin (2004) with an eastward spread of tropospheric temperatures from the Pacific by equatorial waves. Indeed, potential intensity (PI) of tropical cyclones as formulated by Bister and Emanuel (2002) depends on tropospheric temperature. An increase of tropospheric temperature may lead to a higher outflow temperature and a decrease of PI (Ramsay & Sobel, 2011). Vecchi and Soden (2007) and Swanson (2008) found that this effect substantially influences PI in climate projections and observations. It was even anticipated by Vecchi et al. (2008) that a

mean global warming of SST has a smaller impact than that from internal climate variability that tend to induce regional SST anomalies. Zhang et al. (2017) investigated the modulation of tropical cyclone activity in the North Pacific induced by the Atlantic meridional SST mode in a global coupled model. They found that the SST mode modifies the Walker cell which in turn has an impact on tropical cyclones in the Pacific by a change of the vertical wind shear. Therefore, dynamical processes can, besides thermodynamic processes, also contribute to the nonlocality of tropical cyclone activity.

The present study investigates the nonlocality of tropical cyclone activity within an idealized atmospheric circulation model. So far no model study exists in which the nonlocality is simulated with an idealized model setup. However, such experiments can possibly further shed light on the mechanisms. In real data and realistic climate projections, many different events may influence tropical cyclone activity and it is hard to obtain a clear evidence for the nonlocality mechanism. However, in idealized experiment, one can isolate the mechanism by suppressing all other influences than local modification of SST. Here it is prescribed for two idealized continents and oceans in order to see how a modification of SST influences the tropical cyclone activity in remote regions. The study is organized as follows. Section 2 contains a brief model description and the outline of the various model experiments. In section 3, the applied cyclone identification and tracking algorithm are explained. Section 4 presents the results of the performed model simulations; and in section 5, the nonlocality mechanism is analyzed with various diagnostics. Section 6 summarizes the outcome of this study.

2. Model and Experimental Design

2.1. Model Description

For the present study, we employ the PlanetSimulator (PlaSim), which is a spectral climate model for the atmosphere (see Fraedrich et al., 2005) and can be coupled to models for the adjacent climate compartments, viz., land, ocean, land ice, and vegetation. Here PlaSim is used with fixed boundary conditions except for land. All prognostic model variables for the atmosphere are expanded in terms of spherical harmonic functions but a transform method is applied to evaluate nonlinear and diabatic terms in grid point space. For low- and high-resolution setups, we truncate the spectral expansion at total wave number 42 (T42) and 170 (T170), respectively. At spectral resolution T170 (T42), the nonlinear and diabatic terms are evaluated on a 512 $\times$ 256 (128 $\times$ 64) Gaussian grid that has approximately a grid-spacing of 78.125 km (312.5 km) near the equator. The vertical coordinate is σ (pressure divided by surface pressure) and the model uses 28 unequally spaced σ-levels. The model includes parameterization schemes for radiation, microturbulent exchange, convection, and large-scale precipitation. The shortwave radiation scheme by Lacis and Hansen (1974) is applied for the cloud-free atmosphere. The cloudy part, the albedos, and transmissivities are parameterized as described by Stephens (1984). The broad band emissivity method by Sasamori (1968) is used for clear-sky longwave radiation. The longwave cloud flux emissivity is obtained from the cloud liquid water content as described by Stephens (1984). Surface fluxes are calculated with bulk aerodynamic formulas. The associated drag and transfer coefficients depend on Richardson number as described by Louis (1979) and Louis et al. (1982). The formulation of the vertical turbulent exchange coefficient follows a mixing length approach as an extension of the similarity theory used for the surface layer (see Roeckner et al., 1992). For cumulus convection, the parameterization by Kuo (1974) is employed. Large-scale condensation forms precipitation that falls out instantaneously. A more detailed description of the model is given by Lunkeit et al. (2011b).

2.2. Experimental Design

An idealized land-sea distribution composed of two continents and two oceans (see Figure 1) is used to simulate nonlocality effects in tropical cyclone activity. The two continents extend meridionally from 90°S to 90°N, while zonally they reach from 180°W to 90°W and 0°E to 90°E, respectively. The experiments do neither include an annual cycle nor a diurnal cycle and the SST of the two-ocean basins is prescribed with a time-independent field. In the reference run, it is given by

$$T_s = 263.15\mathrm{K} + 40\mathrm{K}\left(1 - \sin^4\varphi\right), \tag{1}$$

where T_s denotes the SST, and φ the latitude. Therefore, at the equator, the SST becomes 30°C and at the poles, −10°C. The sea ice formation is ignored in the performed experiments. This profile reveals a weaker

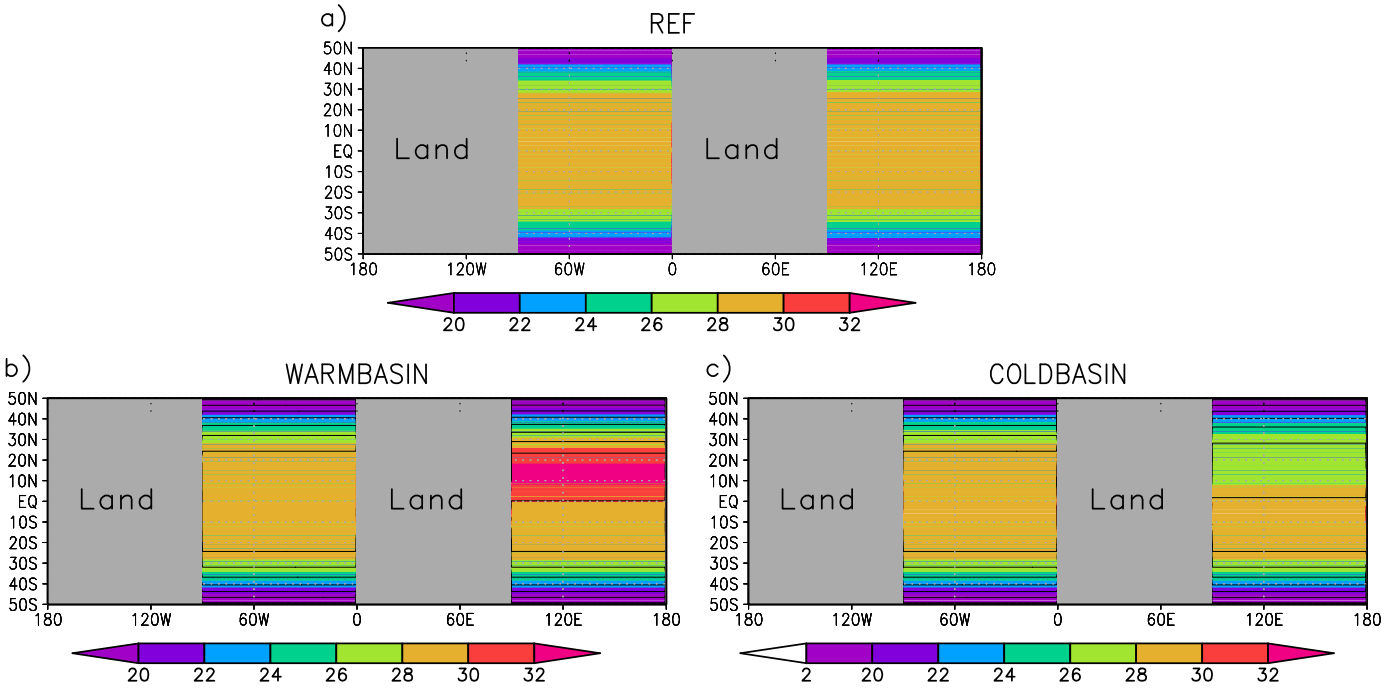

Figure 1. Land-sea distribution and SST (colored shadings and black isolines, contour inverval 2°C) for the experiments (a) REF, (b) WARMBASIN, and (c) COLDBASIN. The land areas are represented by grey shaded areas.

SST gradient in the tropics and a lower SST at the poles compared to idealized aquaplanet simulations of Li et al. (2013) and Ballinger et al. (2015). The former difference yields a larger number of tropical cyclones, while the latter mimics the effect of absent sea ice. The surface temperature and moisture over land are simulated by a one layer soil model (see Lunkeit et al., 2011b). This submodel includes the parameter surface albedo which is set to 0.45. The high value proved to be necessary to avoid too warm land surface temperatures acting to suppress tropical cyclone activity. The albedo increases further in regions with nonzero snow cover. All other land model parameters are set to standard values describing a homogeneous land surface. The parameterization of shortwave radiative transfer does not include ozone since it suppresses tropical cyclones severely in the present model setup. Instead, Newtonian cooling regulates temperature of the five uppermost model levels with a relaxation time of 15 days. The remaining model configuration accords with the default setup of PlaSim (see Lunkeit et al., 2011a).

The model starts from rest for a 10 year simulation at the low-resolution T42 for each individual model experiment. This time period proved to be sufficient for the establishment of a quasi-steady state climate. The final state of this spin-up run forms the initial state of a 5 year simulation at the high-resolution T170. The outcome of the high-resolution run yields the basis of the analysis.

The three experiments REF, WARMBASIN, and COLDBASIN have been performed. The SST given by equation (1) has been used for experiments WARMBASIN and COLDBASIN, including a positive and a negative SST anomaly of 2.5 K in the northeastern basin (Figure 1) for each. The magnitude of the SST anomaly corresponds to a very strong El Nino event in the east Pacific (see e.g., Trenberth, 1997) but is larger than the amplitudes of the Pacific and Atlantic meridional modes (see Chiang & Vimont, 2004). The positive and negative SST anomalies are prescribed by

$$T_s' = \pm 2.5\mathrm{K}\exp\left[-(\varphi-\pi/12)^2/(\pi/12)^2\right] \qquad \text{for } \pi/2 < \lambda < \pi, \tag{2}$$

where λ denotes the longitude. Due to the symmetry of the land-sea distribution, it is irrelevant for the outcome of this study in which basin the anomaly occurs. We also performed two further experiments GLOBALWARMING and GLOBALCOOLING where the SST of REF has been uniformly increased and decreased by 2.5 K, respectively. These experiments reveal how global tropical cyclone activity responds to a uniform SST change in comparison to local SST changes as in WARMBASIN and COLDBASIN.

3. Cyclone Identification and Tracking

Analyzing tropical cyclone activity in the model requires an objective method for the determination of tropical cyclone tracks. The chosen method consists of three steps: Identification, tracking, and filtering. First, all local minima (maxima) of stream function at 1,000 hPa in the Northern (Southern) Hemisphere are identified on the Gaussian model grid. The following criteria must be fulfilled to designate them as convective cyclones (all radii refer to the great circle distance):

1. The stream function value at the local minimum (maximum) must undershoot (exceed) the average values of the surrounding grid points within a certain search radius $\Delta\alpha$ by the increment $\Delta\psi_{\min}$.
2. The maximum horizontal wind speed at 1,000 hPa within the search radius $\Delta\alpha$ is referred to as intensity V_I and must exceed the threshold $V_{\min}$.
3. The magnitude of horizontal wind at 300 hPa averaged over the grid points within the search radius $\Delta\alpha$ is referred to as upper layer wind V_U and must be below the threshold $V_{U\max}$.
4. The convective precipitation rate (the convective precipitation solely results from the convective parameterization scheme and has no contribution from the large-scale precipitation) averaged over the grid points within the search radius $\Delta\alpha$ is referred to as cyclone convective precipitation P_C and must exceed the threshold $P_{C\min}$.

The values for the chosen search radius and threshold parameters are listed in Table 1. The identified convective cyclones do not necessarily occur within the tropical regions because such cyclones can also develop in other regions.

In the next step, the identified convective cyclones are connected to individual cyclone tracks. For this purpose, it is necessary to compare the identified cyclone positions of adjacent 6 hourly output time steps. First, the nearest neighbors of the two time levels are connected if the great circle distance between them does not exceed the tracking radius $\Delta\beta$. Then, the procedure continues with the second nearest neighbors, third nearest neighbors, and so on until the distance becomes larger than $\Delta\beta$. Finally, a filter procedure selects the determined tracks which are designated as hurricane tracks (in this study, the term hurricane refers to all tropical cyclones having the characteristics of Atlantic hurricanes). The procedure adopts the following criteria:

5. The intensity V_I must exceed the threshold $V_{H\min}$ at one or more locations along the cyclone track.
6. The upper layer wind V_U must be below the threshold $V_{U0\max}$ at the location where the cyclone track begins.
7. The cyclone track must begin at a latitude having an absolute value below φ_T.
8. At the time of maximum intensity, a local maximum of 300 hPa temperature must exist within the search radius having the $\Delta\gamma$ and exceed the average 300 hPa temperature of the grid points within the search radius $\Delta\alpha$ by the difference $\Delta T_{U\min}$. The actual value of this temperature excess is referred to as the upper layer temperature anomaly ΔT_U.
9. The cyclone track must at least extend over a time period of $\Delta t_{\min}$.

Table 1 also contains the chosen parameters for the filtering procedure.

Criterion 6 effectuates the exclusion of cyclones generated by baroclinic instability which represents the usual mechanism for extratropical cyclogenesis. The criteria 3 and 4 exclude the identification of cyclones having undergone an extratropical transition. Criteria 5 and 8 ensure that the cyclone adopts the characteristics of a hurricane at least at one location along the cyclone track. Finally, criterion 7 guarantees that the cyclone formed in the tropics. Note that the threshold value for $V_{H\min}$ falls below the value 33 m/s that has to be exceeded to term a tropical cyclone as hurricane according to the Saffir-Simpson scale (Simpson, 1974). This decrease of the wind speed threshold can be justified by the model resolution T170 which leads to a reduced magnitude of inner core wind speed compared to observations (see e.g., Li et al., 2013). Therefore, we assume that tropical cyclones already exceeding 25 m/s would exceed the 33 m/s threshold at a higher model resolution and can be classified as hurricanes.

Table 1
Parameters for the Cyclone Identification and Tracking Routines

Parameter	Value	Parameter	Value
$\Delta\alpha$	5° (≈555 km)	$\Delta\gamma$	2.5° (≈278 km)
$\Delta\psi_{\min}$	0.1 × 10^6 m^2/s	$V_{H\min}$	25 m/s
$V_{\min}$	12 m/s	$V_{U0\max}$	8 m/s
$V_{U\max}$	20 m/s	ϕ_T	30°
$P_{C\min}$	0.36 mm/h	$\Delta T_{U\min}$	1 K
$\Delta\beta$	5° (≈555km)	$\Delta t_{\min}$	24 h

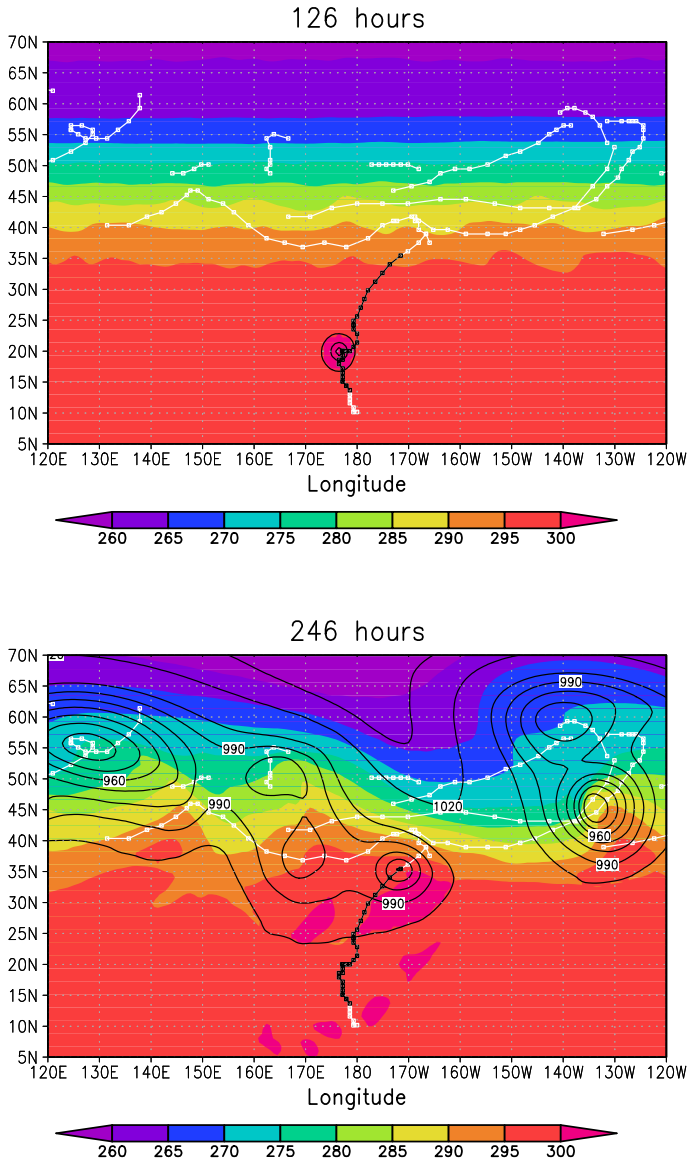

Figure 2. Snapshots of 1,000 hPa temperature (colored shadings, K) and surface pressure (black isolines, contour interval 5 hPa) of the test simulation. Detected cyclone tracks are also shown. The black colored cyclone track emerges when all criteria are applied, while the white colored cyclone tracks form the outcome of cyclone tracking based only on criteria 1, 2, 5, and 9.

We performed an idealized experiment at spectral resolution T170 to test the realism of tropical cyclone representation and the tracking procedure. We run the model in aquaplanet configuration and initialized the model with the analytical tropical vortex as given by Reed and Jablonowski (2011) and added a geostrophically balanced jet stream as described by Polvani et al. (2004). The additional temperature anomaly resulting from thermal wind balance had been found in such a way that the temperature coincides with that prescribed by Reed and Jablonowski (2011) at the equator. The SST of the aquaplanet is identical with the temperature of the atmosphere at the lower boundary. The specific humidity field given by Reed and Jablonowski (2011) is modified by the factor

$$f_q = \frac{1}{2}\{1-\tan[5(\varphi-2\pi/9)]\} \quad \text{for} \quad \varphi > 0, \tag{3}$$

to avoid an excessively large relative humidity at high latitudes. The experiment extending over 15 days describes the genesis and movement of a tropical cyclone that experiences an extratropical transition in the final stage of its life cycle.

Figure 2 shows snapshots of surface pressure and 1,000 hPa temperature together with the detected cyclone tracks. The white colored tracks have been detected by applying only the criteria 1, 2, 5, and 9 while the black colored track results when all criteria are applied. The black colored track is associated with the life cycle of a tropical cyclone reaching hurricane intensity. It becomes extratropical at the location where the black track ends. The latter result is the same when the latitude criterion 7 is ignored. Therefore, the other criteria are already sufficient to isolate the tropical cyclone. Figure 3 shows diagrams in which the cyclone tracks are plotted as functions of the cyclone properties V_l, P_C, ΔT_U, and V_U. It becomes clear that the tropical cyclone track begins at some distance north of the initial perturbation position since the convective precipitation P_C is below the threshold $P_{C\min}$ south of this position (Figure 3a). This is due to the spin-up of the idealized initial vortex that has unlike real tropical depressions no convective clouds. The tropical cyclone track ends because the upper layer wind V_U exceeds the threshold $V_{U\max}$ due to criterion 3 (Figure 3b). All but one shown extratropical cyclones do not fulfill criterion 6. Therefore, initial upper level wind is a suitable quantity to distinguish tropical cyclones from extratropical ones. The diagram 3b has some similarity with the cyclone phase space by Hart (2003). Indeed, the coordinate axes have similar meaning and the extratropical transition also manifests in a trajectory curving left hand into the upper left part of the diagram. The criterion 3 removes the part of the cyclone life cycle after extratropical transition and this is intended since we wish to exclude extratropical cyclones in our analysis.

4. Results

Before performing the simulations at high resolution, we have checked whether the model has attained a steady state climate after 10 years simulation at low resolution. Suitable indicators for the steady state climate are globally averaged surface temperature and moisture content in the atmosphere. Figure 4 shows the time series of these quantities for the experiments REF, WARMBASIN, and COLDBASIN. The averaged surface temperature and the atmospheric moisture content have reached a quasi-steady state after 3 years in all the experiments. The WARMBASIN run yields as expected the highest surface temperature, while the COLDBASIN run has the coldest surface on average. The globally averaged moisture content has similar values for REF and

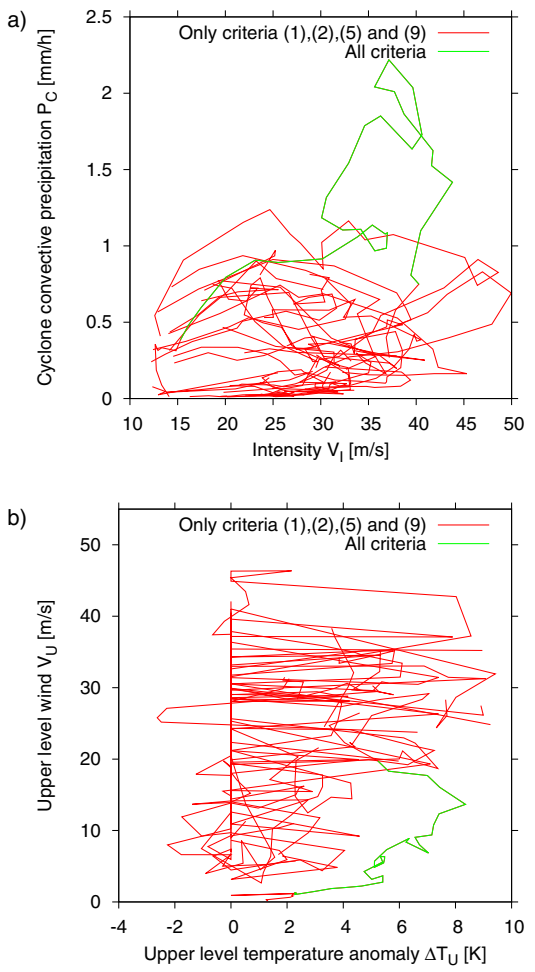

Figure 3. Phase diagrams for cyclone properties along the tracks showing (a) intensity V_I versus cyclone convective precipitation P_C and (b) upper level temperature anomaly ΔT_U versus upper level wind V_U. The green colored curve refers to the cyclone track emerging when all criteria are applied while the red colored curves result from cyclone tracking based only on criteria 1, 2, 5, and 9.

COLDBASIN and is significantly larger for WARMBASIN. Therefore, the response of the moisture content to SST is manifested in a nonlinear way. After 10 years, the model runs for five further years with increased resolution T170 which may change the climate state. However, the higher resolution yields a similar globally averaged surface temperature. On the other hand, the globally averaged moisture content of REF and COLDBASIN experiences an abrupt decrease at higher resolution. Despite this change, a rapid transition to a quasi-steady state takes place in these experiments. Therefore, we use the complete 5 years of the high-resolution run for our analysis.

Figure 5 shows the detected hurricane tracks of the three experiments. In experiment REF, hurricane tracks appear in all four basins with similar frequencies while large differences in frequency can be observed in the two sensitivity experiments. A clustering of tracks can be seen in the western part and to a lesser extent in the eastern part of the basins in REF. A huge number of hurricane tracks appear in the northeastern basin whereas no or only few hurricanes have developed in the other basins in WARMBASIN. The situation is reverse in COLDBASIN where no hurricanes developed in the northeastern basin while many occur in the other basins. The hurricane tracks displayed here already signify a nonlocality effect in tropical cyclone activity. Figure 5 also displays the intensity of the tropical cyclones along the tracks in terms of the Saffir-Simpson scale, and the numbers of tracks for each category are listed in Table 2. Obviously, the tropical cyclones rarely reach the intensity of a named hurricane and has exceeded category 2 once only in all the simulations due to the spectral model resolution of T170. Li et al. (2013) found with a spectral model in aquaplanet simulations that the number and intensity of simulated tropical cyclones increases with model resolution. Although they adopt a lower SST in their model, they detect at a resolution of T170 that per year about 12 tropical cyclones reach category 1 while less than one reach category 3 on average. The higher amount of named hurricanes in their simulations could result from the different experimental setup or the different parameterization schemes for subgrid-scale processes. The presence of continents in our simulation could also have a weakening effect that needs to be investigated in a comparison study. PlaSim has also been tested at spectral resolution T170 with observed land-sea distribution, SST and orography (Abdullah, 2015). A 1 year simulation reveals a realistic number of 47 hurricane tracks per year and also a realistic distribution in the various ocean basins.

The accumulated cyclone energy (ACE) index by Bell et al. (2000) represents a suitable measure for tropical cyclone activity. It is given by

$$ACE = \sum_{n=1}^{N} \left(\frac{V_{In}}{100\ \mathrm{m/s}} \right)^2, \tag{4}$$

where the index n is a counter for all detected cyclones of the various hurricane tracks in a certain basin. Table 3 contains the ACE values together with the number of hurricane tracks for the various basins. The values in the table show that the ACE index per annum is roughly similar to the number of tropical cyclone tracks of the five simulation years. We can deduce a severe increase and decrease of tropical cyclone activity in the ocean basin with modified SST in WARMBASIN and COLDBASIN, respectively. In WARMBASIN, the ACE index increased by more than a factor 8 while in COLDBASIN the ACE index becomes marginal. The nonlocal response is similarly significant in WARMBASIN where the ACE index is either zero or marginal in the unmodified ocean basins. There is also a nonlocality effect in COLDBASIN where the ACE index increased by factors between 1.4 and 2.5 in the remote basins. However, the strength of nonlocality is

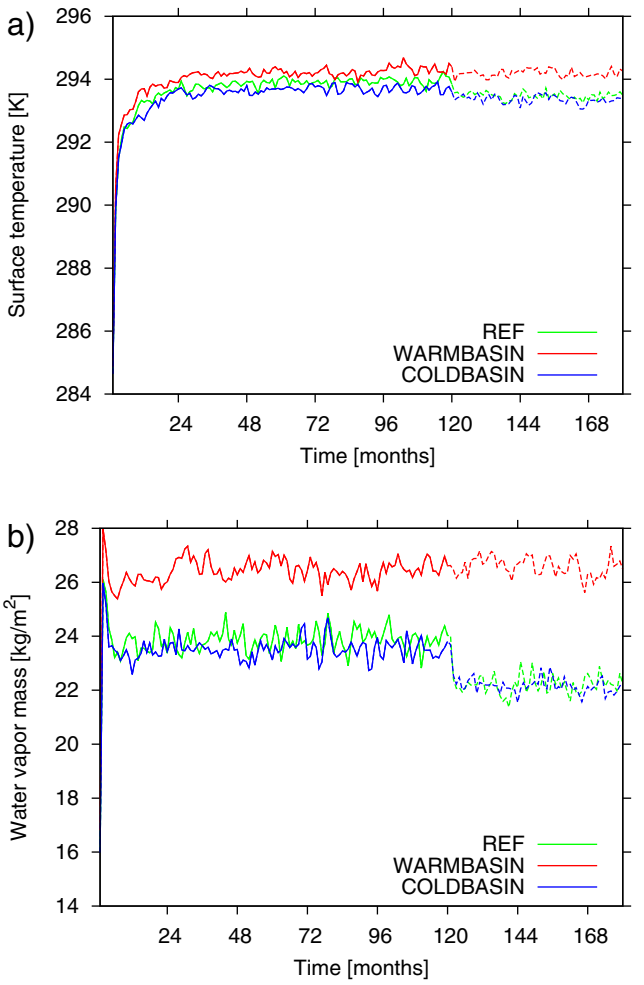

Figure 4. (a) Globally and monthly averaged surface temperature (K) and (b) globally and monthly averaged atmosphere water vapor content (kg/m^2) as a function of time for the various experiments. Note that the spectral resolution changes from T42 (solid lines) to T170 (dashed lines) after 120 months.

weaker as in WARMBASIN. This result should be compared with the findings of Sobel et al. (2002) that the region with highest SST governs the tropical tropospheric temperature. Then, a change of tropical cyclone activity due to the tropical tropospheric temperature effect should only result in experiment WARMBASIN. The ACE index increases in experiment COLDBASIN as revealed by Table 3 cannot be explained in this way and must stem from other mechanisms. Figure 6 shows the annual ACE index for each simulated year. There is an interannual variability of the ACE index. However, the property that the ACE index of the remote basis is lower in experiment WARMBASIN and is higher in experiment COLDBASIN is valid for each year except for the southwestern basin where REF has a higher ACE index than in COLDBASIN for the last 2 years. However, the ACE index in REF is anomalously high in these years compared to the other basins. Therefore, a long-term average should yield a result consistent with the 5 year average due to the basin symmetry in experiment REF.

Table 4 shows the global values for the ACE index and number of tropical cyclone tracks. We see that both quantities rise in the perturbation experiments WARMBASIN and COLDBASIN. Furthermore, the response is also stronger than in the global change experiments GLOBAL WARMING and GLOBAL COOLING. Therefore, the model suggests in agreement with Vecchi et al. (2008) that a uniform change of SST has a smaller impact on tropical cyclone activity than a regional change with the same amount. The nonmonotonic dependency of ACE on globally uniform SST changes appears peculiar. On the other hand, the ACE difference between REF and GLOBAL COOLING is only 6.4 and the annual standard deviation of ACE ranges between 22.3 and 34.1 in the various experiments with uniform SST perturbations. Therefore, the difference is likely not statistically significant. The small sensitivity to uniform SST perturbations probably appears due to compensation of factors that enhance tropical cyclones and other that hamper them. Such a circumstance has been found by Emanuel (2013) in global warming projections by CMIP5 climate models which show an increase in potential intensity but also an increase of the inhibiting saturation deficit. However, analyzing the reasons for the global response is not the purpose of this study and, therefore, will not be considered further.

5. Analysis

In order to find the reasons responsible for the strong nonlocality response in the model, we analyze the seasonal genesis parameter (SGP) by Gray (1979) and the genesis potential index (GPI) by Emanuel (2010a) from monthly averaged model output. The SGP results from the following formula

$$\mathrm{SGP}=30\underbrace{|f|(\zeta_{950}\times 10^{6}\mathrm{s}^{-1}+5\mathrm{s}^{-1})(|\mathbf{v}_{200}-\mathbf{v}_{950}|+3\mathrm{m/s})^{-1}}_{\text{Dynamic potential}}$$
$$\underbrace{(T_s-299.15\mathrm{K})(\theta_{e1000}-\theta_{e500}+5\mathrm{K})\frac{H_{700}+H_{500}-0.8}{0.6}}_{\text{Thermodynamic potential}}=S_1S_2S_3S_4S_5S_6, \quad (5)$$

where f denotes the Coriolis parameter, ζ the relative vorticity, $\mathbf{v}$ the horizontal wind vector, θ_e the equivalent potential temperature, and H the relative humidity. The indices refer to the pressure in hPa on the respective pressure surface where the field quantity is evaluated. The parameter composed of six factors predicts that tropical cyclogenesis takes place preferentially in regions with high Coriolis-parameter (factor S_1), high low-level vorticity (factor S_2), weak vertical wind shear (factor S_3), high SST (factor S_4), high

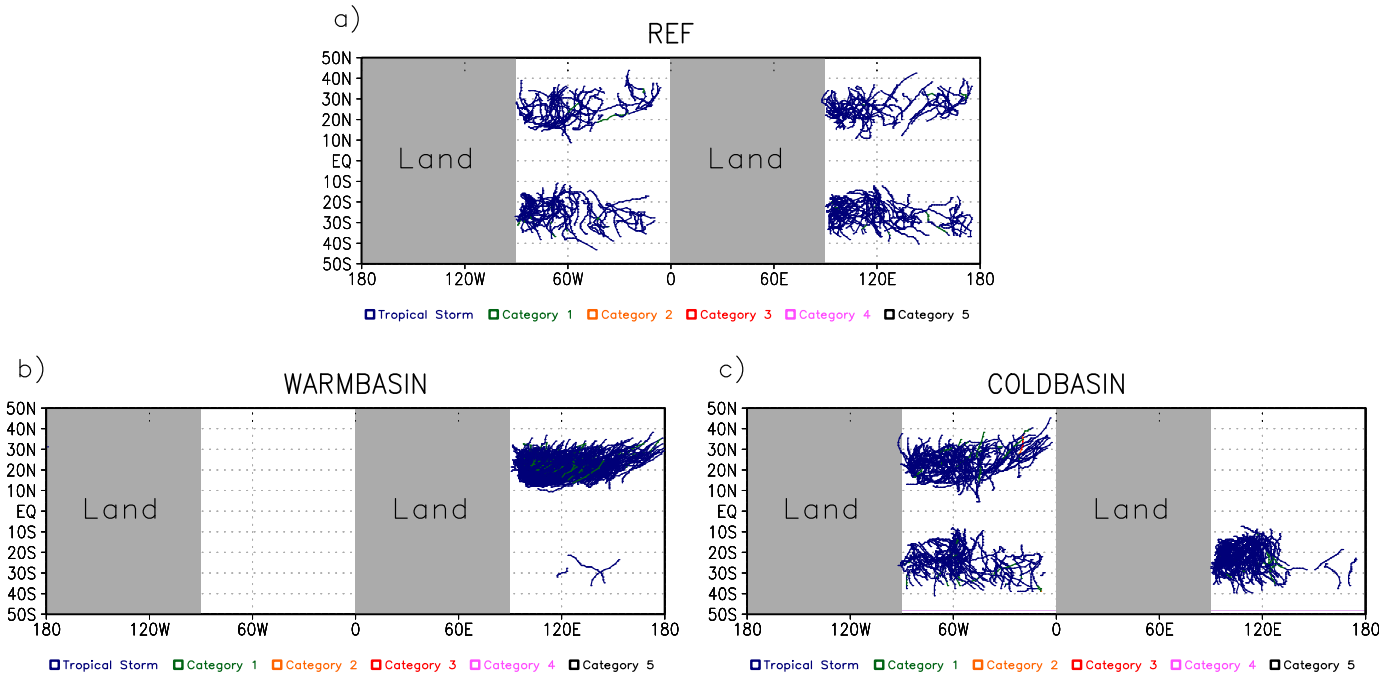

Figure 5. Detected hurricane tracks in the experiments (a) REF, (b) WARMBASIN, and (c) COLDBASIN. The color indicates intensity according to the Saffir-Simpson scale (see legend) and continents are masked with grey color.

moist convective instability (factor S_5), and high relative humidity (factor S_6). The SGP indicates impossibility of tropical cyclogenesis in regions where the sea surface temperature T_s is below 299.15 K, the mean relative humidity $(H_{700}+H_{500})/2$ is below 40%, the relative vorticity ζ_{950} is anticyclonic with a magnitude of more than $5 \times 10^{-6}\,\mathrm{s}^{-1}$, and the vertical moist static stability parameter $\theta_{e500}-\theta_{e1000}$ is above 5 K.

The GPI composed of four factors is given by

$$\mathrm{GPI}=10^5|f+\zeta_{850}|^3\left(\frac{s_b-s_m}{s_o^*-s_b}\right)^{-4/3}\left(V_{pot}-35\mathrm{m/s}\right)^3\left(|\mathbf{v}_{200}-\mathbf{v}_{850}|+25\mathrm{m/s}\right)^{-4}=G_1G_2G_3G_4, \tag{6}$$

where V_{pot} is the potential intensity (PI) as defined by Bister and Emanuel (2002) and s_b, s_m, and s_o^* denote the specific moist entropies of the boundary layer, 500 hPa, and the sea surface, respectively. The term in brackets of the second factor G_2 represents the saturation deficit of the middle troposphere which obstructs tropical cyclogenesis. The GPI has in contrast to the SGP no fixed threshold in sea surface temperature and in relative humidity (factor G_3). However, the GPI becomes zero in regions where the absolute vorticity $f+\zeta_{850}$ is anticyclonic (factor G_1) and the potential intensity falls below 35 m/s (factor G_3). The GPI as given by (6) is an improved formulation of the original version by Emanuel and Nolan (2004) and turned out to be a better predictor for tropical cyclone activity (Camargo et al., 2014). The GPI should also be a better indicator for tropical cyclone activity in variable climates compared to the SGP because the threshold value 299.15 K is likely only reasonable for present climate conditions.

Table 2
Number of Tropical Cyclones in the Various Intensity Classes According to the Saffir-Simpson Hurricane Scale for the Experiments REF, WARMBASIN, and COLDBASIN

	Tropical storm	Category 1	Category 2	Category 3	Category 4	Category 5
REF	193	14	0	0	0	0
WARMBASIN	264	46	0	0	0	0
COLDBASIN	227	31	1	1	0	0

Table 3
ACE Index Per Annum (First Number) and Number of Detected Tropical Cyclone Tracks (Second Number) in the Various Ocean Basins for the Experiments REF, WARMBASIN, and COLDBASIN

	REF		WARMBASIN		COLDBASIN	
	West	East	West	East	West	East
North	38.1/43	42.4/52	0/0	330.0/307	96.5/97	0/0
South	50.0/51	54.2/61	0/0	1.6/3	69.3/64	88.2/99

The indicators include various physical quantities for predicting the frequency of tropical cyclones. To find out which of these are relevant for the changes in the model simulations, it is necessary to calculate the various contributions. By noting that both indicators can be written as

$$Y=\prod_{n=1}^{N} X_n, \tag{7}$$

where the X_n denote the various factors and Y the indicator, it is reasonable to estimate the importance of one factor by calculating its contribution in a Taylor expansion up to the linear order, namely,

$$\Delta Y \approx \sum_{n=1}^{N} \frac{\partial Y}{\partial X_n} \Delta X_n = \sum_{n=1}^{N} \left(\prod_{n' \neq n} X_{n'} \right) \Delta X_n. \tag{8}$$

Each summand yields the linear contribution to the change due to the respective factor.

Figure 7 displays the SGP together with the genesis locations for the experiments REF, WARMBASIN, and COLDBASIN. In REF, the SGP maximizes slightly poleward of the latitude 20°N or 20°S in each basin and the largest maximum arises in the western part of the basins while a weaker secondary maximum is located in the eastern part of the basin. This is consistent with the clustering of tracks seen in Figure 5. The maximum in the western part results to a high degree from the vorticity factor S_2 while in the eastern part the weak vertical shear and low convective instability contribute mainly to the local maximum (not shown). In most cases, genesis takes place at locations where the SGP is nonzero. In WARMBASIN, the SGP is greatly increased in the warmed ocean basin while in the other basins, a nonzero SGP can only be found in the western part. Furthermore, the maximum occurs in the western basins equatorward of the maxima in REF at the latitudes 10°N and 10°S. In COLDBASIN, the SGP becomes zero nearly everywhere in the cooled basin while in the other basins the SGP pattern remains similar to REF. The differences to REF reveal a dipole pattern in the remote basins of experiment WARMBASIN due to the equatorward shift. A decrease of SGP arises in a zonal band between 20° and 30° of latitude while the positive anomaly maximizes at the western boundary at about 10° of latitude. Experiment COLDBASIN shows rather unstructured positive and negative responses in SGP in the remote basins.

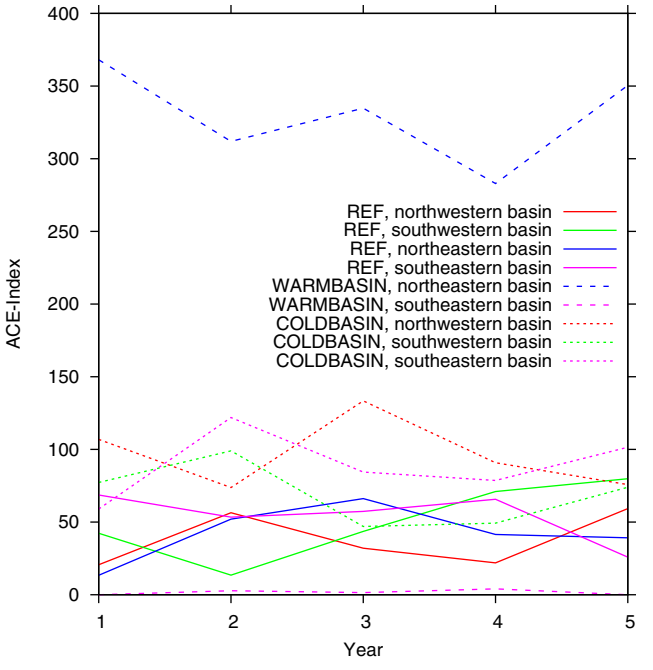

Figure 6. Annual ACE index for the various experiments and basins as a function of the simulated year.

Figure 8 shows fields of the GPI for the three experiments. The GPI fields in REF resemble those of the SGP but the maximum in the eastern part of the basin is more pronounced than in the SGP fields. Surprisingly, the GPI response is negative in the northeastern basin of experiment WARMBASIN although the sea surface temperature is higher and the number of tropical cyclone tracks attains a very large value there. Therefore, the GPI fails to make a reasonable prediction of tropical cyclone activity. The response in the other basins of experiment WARMBASIN agrees with the detected nonlocality of tropical cyclone activity. In experiment COLDBASIN, the decrease of GPI in the northeastern basin accords as for the SGP fields with the change of

Table 4
ACE Index Per Annum and Number of Detected Tropical Cyclone Tracks for the Experiments REF, WARMBASIN, COLDBASIN, GLOBAL WARMING, and GLOBAL COOLING

	REF	WARMBASIN	COLDBASIN	GLOBAL WARMING	GLOBAL COOLING
ACE	184.7	331.6	254.0	237.3	191.1
Number	207	310	260	241	223

tropical cyclone activity. However, the response in the other basins of experiment COLDBASIN does not confirm the nonlocality effect observed by the ACE index and storm counts.

We see that both cyclogenesis indices have deficiencies in predicting the tropical cyclone activity in the sensitivity experiments. To reveal the possible reasons for these deficiencies, we have analyzed various contributions to these indices. Figure 9 shows the linear contributions due to the various factors in the SGP. The factor S_1 of the SGP does not yield any contribution since the Coriolis parameter remains constant. Therefore, this factor has not been considered in the analysis. The vorticity factor predicts in agreement with the analyzed ACE index an increase (decrease) of tropical activity in the northeastern basin and a decrease (increase) in the remote basins for experiment WARMBASIN (COLDBASIN) except for the southeastern basin where the contribution in COLDBASIN is rather slightly negative. The shear factor appears to be mainly responsible for the equatorward shift of the SGP in experiment WARMBASIN (cf. Figure 7d). However, the shear factor shows little remote response in COLDBASIN. The ocean factor has only a contribution in the modified ocean basin since it is only a function of sea surface temperature. This factor is consistent

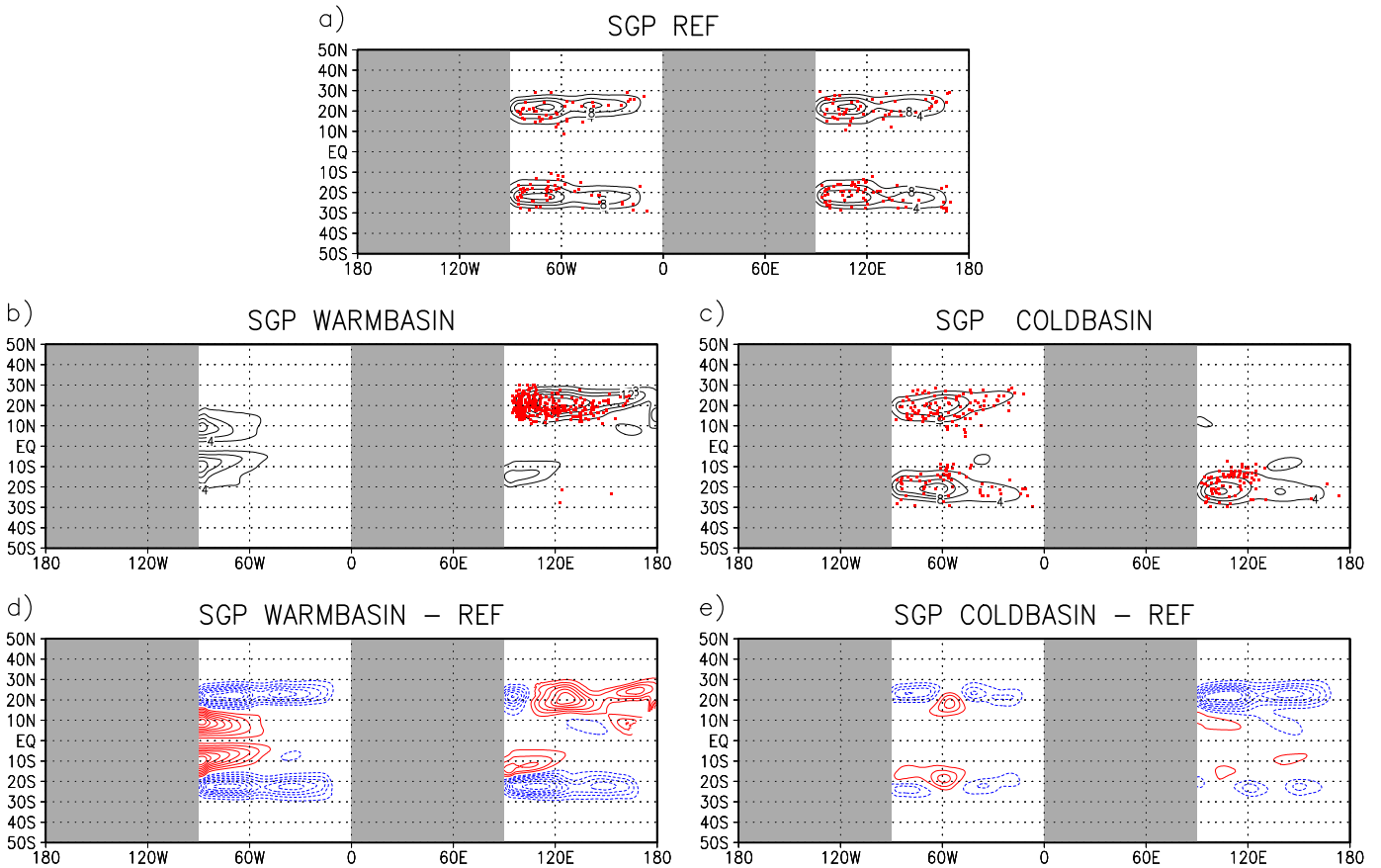

Figure 7. Horizontal fields of the SGP averaged over the last five simulation years for (a) experiment REF, (b) experiment WARMBASIN, (c) experiment COLDBASIN, (d) the difference WARMBASIN–REF, and (e) the difference COLDBASIN–REF. The contour interval is 4 and 2 in Figures 7a–7c and 7d and 7e, respectively. The zero contour has been omitted and continents are masked with grey color. The red dots in Figures 7a–7c mark the positions where the detected hurricane tracks start.

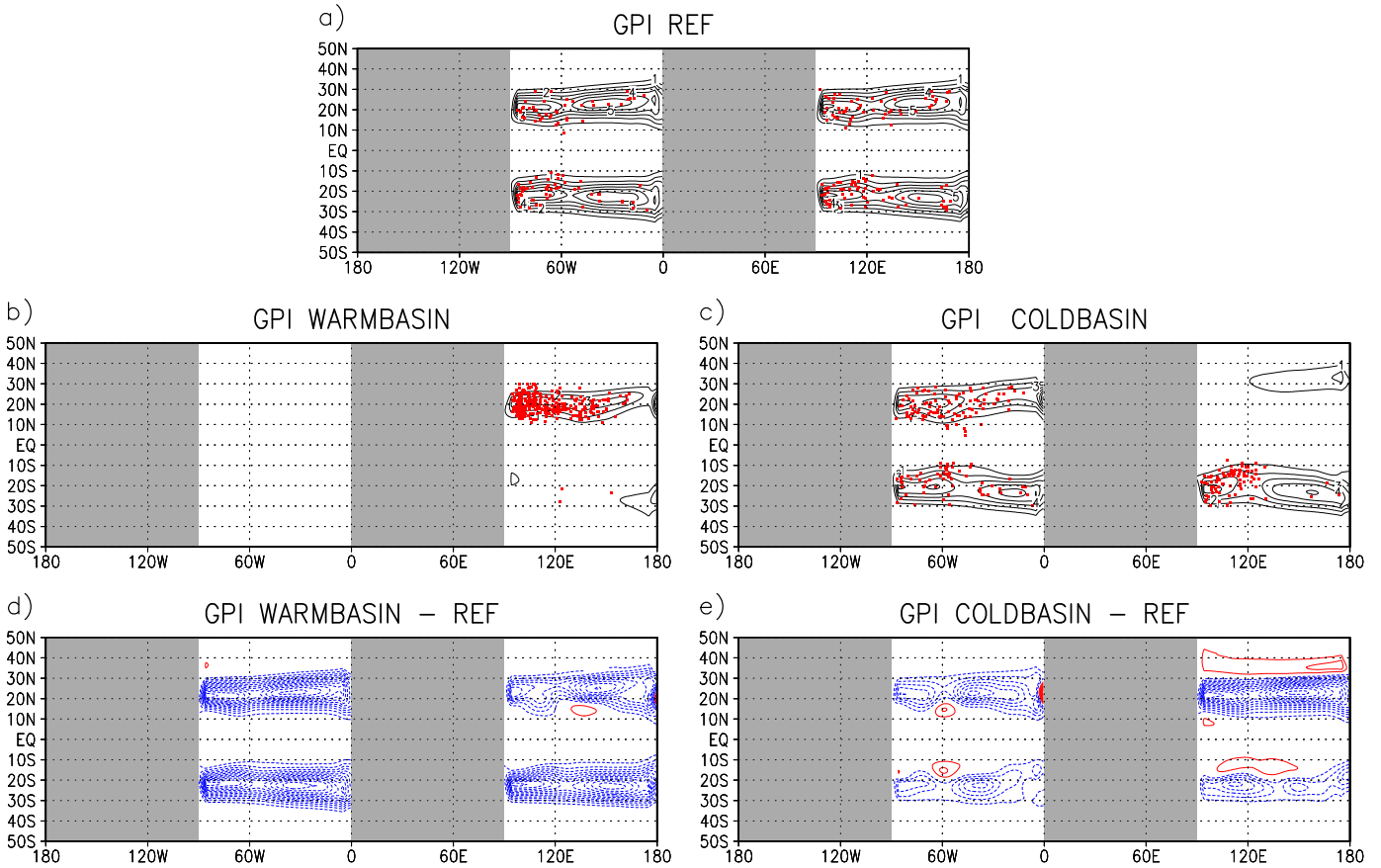

Figure 8. As in Figure 7 but for the GPI. The contour interval is 1 in all plots.

with the change of tropical cyclone activity in the northeastern basin. The stability factor reveals a convective destabilization of the western basin part in the experiment WARMBASIN. This controverts the nonlocal response in tropical cyclone activity but is in agreement with the local change in the northeastern basin. On the other hand, COLDBASIN simulates only a negligible change of convective instability in the regions with enhanced SGP. The humidity factor contribution agrees with the nonlocal response in WARMBASIN but the opposite is true in experiment COLDBASIN. There is a decrease of relative humidity in all basins and in both sensitivity experiments except the southeastern basin of experiment COLDBASIN. This result explains the decrease in SGP in the western part of the modified basin of experiment WARMBASIN.

Figure 10 displays various linear contributions to the changes of the GPI. We see a similar pattern for the vorticity factor contribution as for the SGP but the amplitude is somewhat smaller in experiment COLDBASIN. A stronger contribution results from the humidity factor that yields an increase of saturation deficit at most locations. It explains to a large degree the decrease of GPI in the western part of the modified basin of experiment WARMBASIN. Therefore, the humidity factor turns out to be misleading for predicting tropical cyclone activity in this basin. The contribution of the PI-factor is strong and in agreement with the nonlocal response in experiment WARMBASIN. This result can only be explained by an increase of outflow temperature since the SST is identical in the remote basins of WARMBASIN and REF. In the modified basin of WARMBASIN, a decrease of PI appears in the region with enhanced tropical cyclone activity. Therefore, the PI increase due to the positive SST anomaly is more than offset by the higher outflow temperature. Experiment COLDBASIN reveals a negative contribution of the PI factor in the modified basin but in the other basins no visible change appears. Therefore, the nonlocal response cannot be explained with a change of PI in experiment COLDBASIN. This result agrees with Sobel et al. (2002) who stated that the tropical tropospheric temperature results mainly from the region having the highest SST. The shear factor has positive and negative contributions as for the SGP.

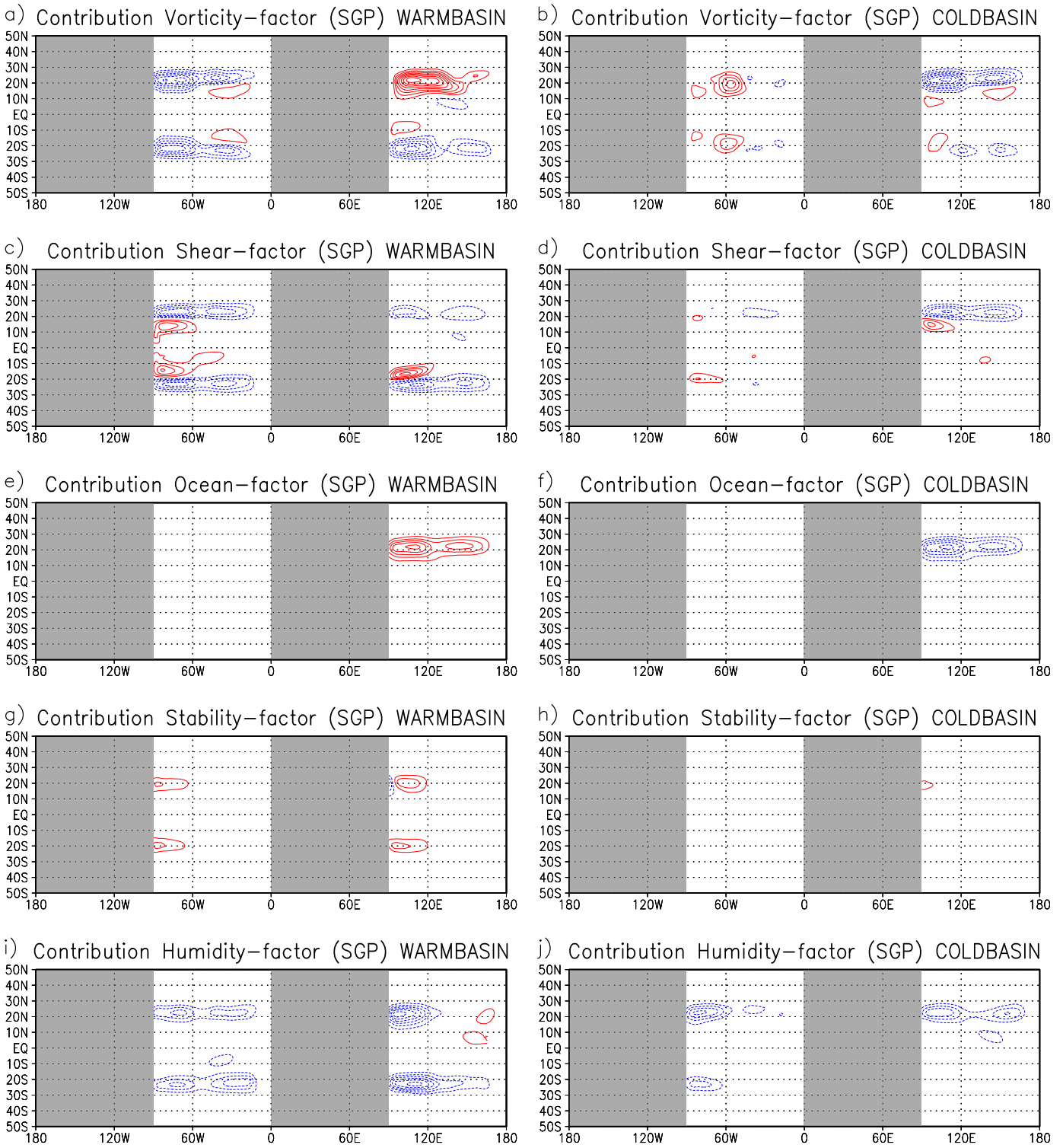

Figure 9. Contributions of the various factors to the SGP difference (left) between WARMBASIN and REF and (right) between COLDBASIN and REF. (a, b) Contributions of the vorticity factor S_2, (c, d) contributions of the vertical shear factor S_3, (e, f) contributions of the ocean factor S_4, (g, h) contributions of the stability factor S_5, and (i, j) contribution of the relative humidity factor S_6. Positive and negative contours are colored in red and blue, respectively. The contour interval is 2, the zero contour has been omitted and continents are masked with grey color.

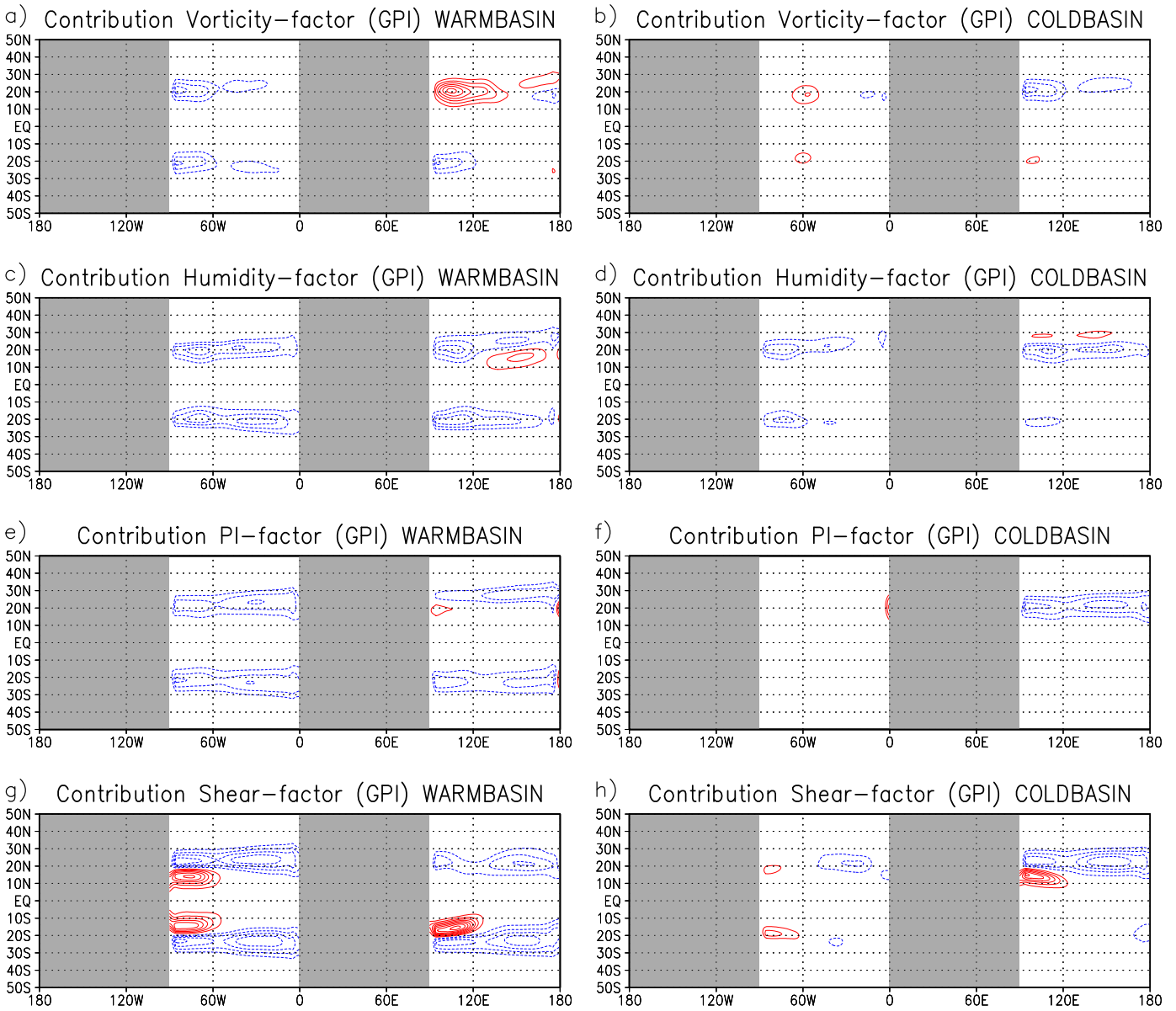

Figure 10. Contributions of the various factors to the GPI difference (left) between WARMBASIN and REF and (right) between COLDBASIN and REF. (a, b) Contributions of the vorticity factor G_1, (c, d) contributions of the humidity factor G_2, (e, f) contributions of the PI factor G_3, and (g, h) contributions of the shear factor G_4. Positive and negative contours are colored in red and blue, respectively. The contour interval is 2, the zero contour has been omitted and continents are masked with grey color.

In summary, we can assert that both cyclogenesis indices cannot entirely predict the sensitivity of simulated tropical cyclone activity to SST anomalies in remote basins. However, we found a consistent contribution by the vorticity factor while the humidity and PI factors are in agreement only in experiment WARMBASIN. The GPI even fails in the prediction of the local response in WARMBASIN, the reason being that the humidity and PI factor contributions do not agree with the found response.

The meaning of vorticity for the TC activity response can possibly be understood in terms of the marsupial paradigm proposed by Dunkerton et al. (2009). They found that tropical cyclones often develop in troughs of tropical waves. These troughs contain a pouch region where the deformation by the horizontal flow field is very weak. Then, an ideal environment for tropical cyclone formation exists if SST, relative humidity, and moist convective instability are high enough. A useful diagnostic for pouch regions is the Okubo-Weiss parameter given by

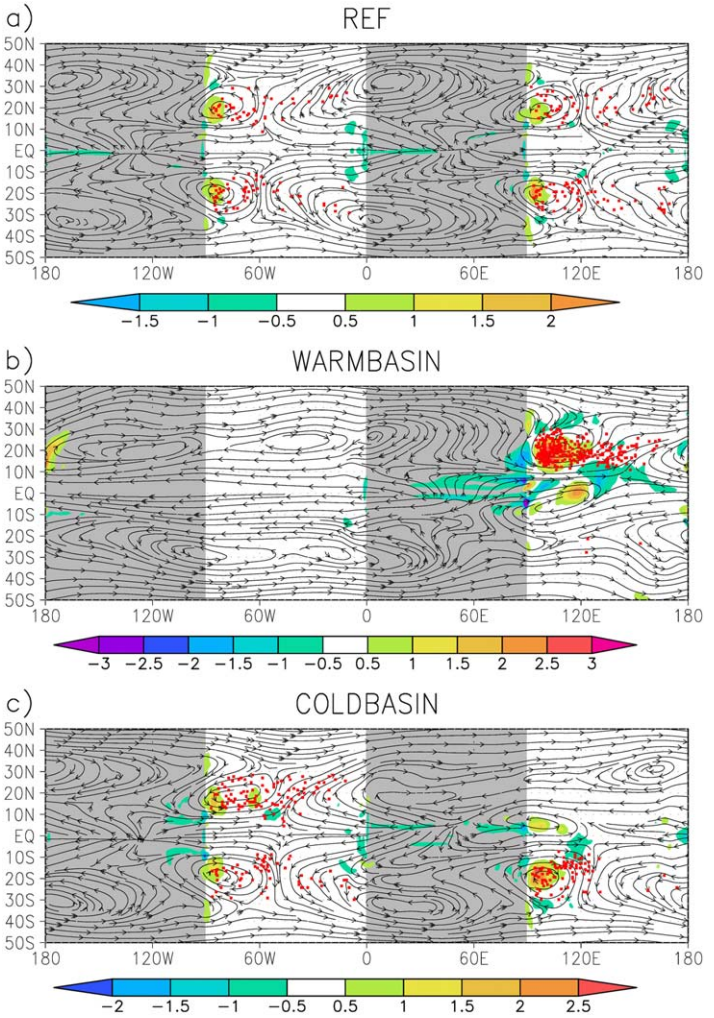

Figure 11. Okubo-Weiss parameter (colored shadings, unit 10^{-10} s^{-2}) and streamlines of the 700 hPa flow averaged over the five simulation years for (a) experiment REF, (b) experiment WARMBASIN, and (c) experiment COLDBASIN. The red dots mark the positions where the detected hurricane tracks start and continents are indicated by grey shading.

$$OW = \left(\frac{\partial v}{\partial x} - \frac{\partial u}{\partial y}\right)^2 - \left(\frac{\partial u}{\partial x} - \frac{\partial v}{\partial y}\right)^2 - \left(\frac{\partial v}{\partial x} + \frac{\partial u}{\partial y}\right)^2, \quad (9)$$

where u and v denote the velocity components of the local Cartesian system having the coordinates x and y. The first summand of the Okubo-Weiss parameter is identical to relative vorticity squared while the other two describe deformations. A high Okubo-Weiss parameter results for a cyclonic solid body rotation, i.e., $u = -cy$ and $v = cx$. Then, the deformation terms disappear. On the other hand, a pure shear flow given by $u = -cy$, $v = 0$ yields a vanishing Okubo-Weiss parameter since the vorticity and deformation terms are offset against each other. Figure 11 displays the time-averaged Okubo-Weiss parameter together with the streamlines of the 700 hPa flow. Indeed, we see that the basins with substantial tropical cyclone activity stand out with a region where the Okubo-Weiss parameter exhibits high positive values while such regions are absent in the basins where no or very few tropical cyclones develop. Closed streamlines revealing cyclonic flow surround these regions. It can be anticipated that cyclogenesis takes place preferentially at the center of these large-scale stationary cyclones. This is indeed true in experiment WARMBASIN where nearly all tropical cyclones develop in the region with enhanced Okubo-Weiss parameter. However, tropical cyclogenesis occurs also quite often east of the large-scale low where the streamlines converge. This convergent flow pattern is absent in the basins without noteworthy tropical cyclone activity. This flow configuration has some similarity with the monsoon trough that represents the favorable large-scale flow pattern for the formation of typhoons in the west Pacific (e.g., Feng et al., 2014). Figure 11 suggests that the large-scale flow pattern causes to a noteworthy degree the magnitude of tropical cyclone activity in the present simulations.

Now, the question comes up why does the impact of SST anomalies on the large-scale flow pattern arise? A change of the SST changes the convective activity in the modified basin. This in turn leads to a modification of the longitudinal overturning circulation which is known as the Walker circulation. The altered Walker circulation has influence on the flow pattern and on the tropical cyclone activity in the remote basins. Velocity potential represents a suitable quantity to diagnose the Walker circulation. Figure 12 shows the time-averaged 200 hPa velocity potential for the three experiments REF, WARMBASIN, and COLDBASIN. A wave number 2 pattern arises in experiment REF where divergence of the 200 hPa flow prevails over the ocean basins. Therefore, two Walker cells exist with upwelling over oceans and downwelling over continents. The velocity potential of the experiment WARMBASIN resembles more that of the real atmosphere (see e.g., Tanaka et al., 2004). In this experiment, we see an upwelling center over the warmed basin while a broad area with flow convergence appears between 120°W and 60°E. In this experiment, the warmed basin plays the role of the West Pacific where also upwelling prevails in summer (see Tanaka et al., 2004, Figure 1). (Note that Tanaka et al. (2004) define velocity potential with the opposite sign. Here, we define velocity potential in such a way that the Laplacian of velocity potential yields the divergence.) Experiment COLDBASIN reveals a less dramatic change of the velocity potential pattern. However, no minimum of 200 hPa velocity potential can be found in the cooled basin anymore. The velocity potential response becomes clearer by considering the difference to REF (Figures 12d and 12e). Indeed, these differences reveal subsidence and ascent above the remote basins in experiments WARMBASIN and COLDBASIN, respectively. The amplitude of the response is higher in WARMBASIN than in COLDBASIN which is in accordance with the weaker nonlocality effect in the latter experiment. This outcome agrees with Zhao and Held (2012) who found a positive correlation between 500 hPa vertical velocity and changes in storm frequency in climate projections.

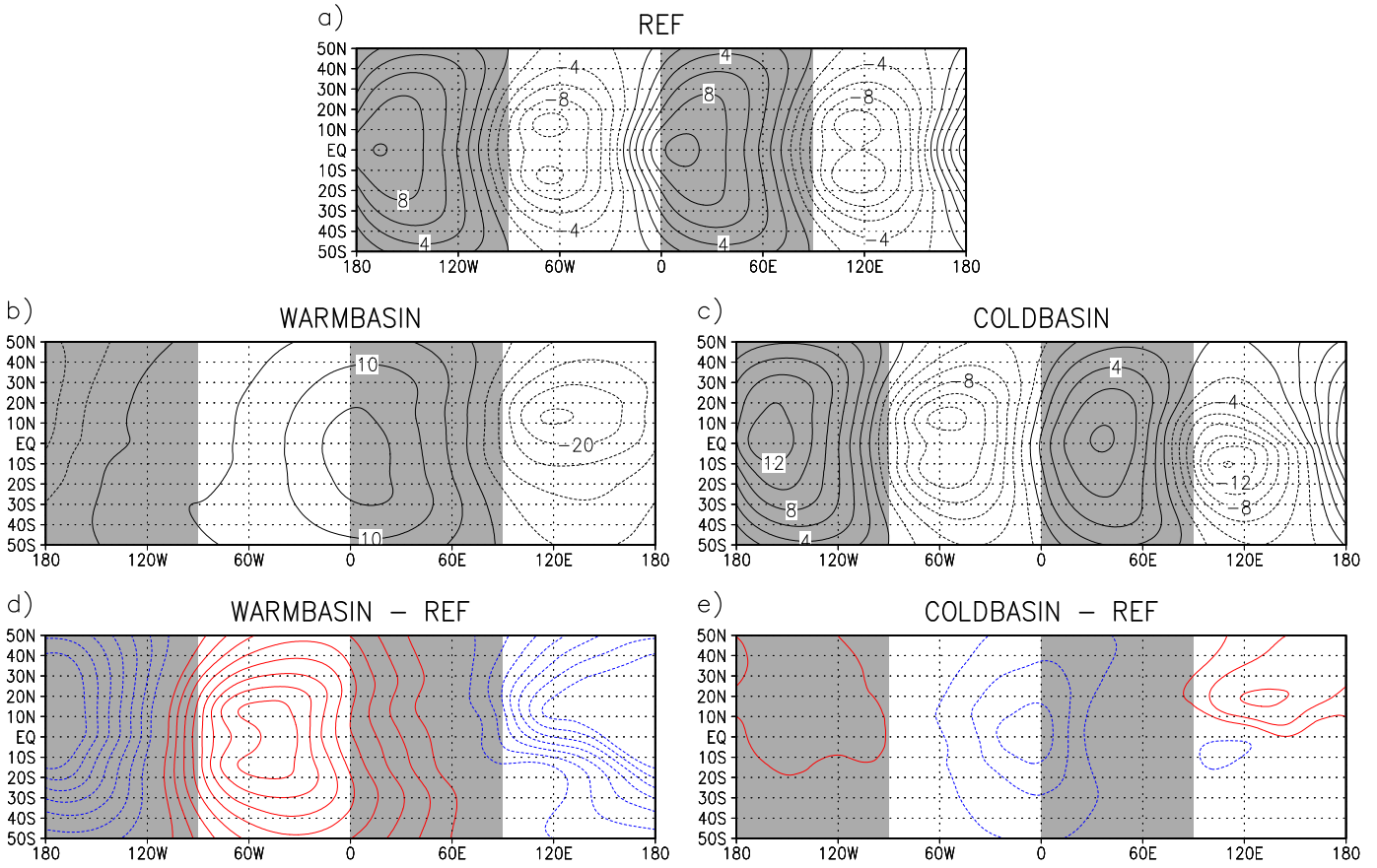

Figure 12. Time-averaged 200 hPa velocity potential (contour interval 2×10^6 s^{-2}) averaged over the five simulation years for (a) experiment REF, (b) experiment WARMBASIN, (c) experiment COLDBASIN, (d) difference between WARMBASIN and REF, and (e) difference between COLDBASIN and REF. In Figures 12d and 12e, positive and negative contours are colored in red and blue, respectively. Negative isolines are dashed and the zero contour has been omitted in Figures 12d and 12e. Continents are indicated by grey shading.

6. Conclusions

In this paper, nonlocality of tropical cyclone activity has been studied for the first time in idealized model experiments. An idealized setup with two continents and two interjacent oceans has been used for the experiments with the atmospheric climate model PlaSim. In the reference experiment, the meridional SST profiles of the two ocean basins are identical (experiment REF) while for experiment WARMBASIN (COLDBASIN), the Northern Hemisphere basin of the eastern ocean includes a warm (cold) SST anomaly up to 2.5 K. Both experiments reveal a significant nonlocality effect, i.e., the ACE index in the unmodified ocean basins changes contrary to the SST anomaly. Therefore, relative SST is a better indicator for TC activity than absolute SST. Indeed, a global warming and global cooling of the SST by 2.5 K lead to a weaker change of tropical cyclone activity in the various basins.

Analyses of the well-known cyclogenesis indices SGP and GPI do not lead to a clear explanation for the nonlocality. However, both indicators reveal a response in accordance with the nonlocality in the experiment WARMBASIN. Here the increase of outflow temperature, decrease of vorticity, and decrease of relative humidity could contribute to the nonlocality. On the other hand, the vorticity change can only consistently explain the nonlocality effect in experiment COLDBASIN. The PI response is in agreement with the finding by Sobel et al. (2002) that the basin with the highest SST controls the tropospheric temperature. Therefore, no change of tropical cyclone activity should occur in the remote basins of experiment COLDBASIN following this argument. At least the weaker nonlocality observed in COLDBASIN supports this hypothesis partly. The consistent response of the vorticity factor suggests that change of large-scale circulation pattern also influences tropical cyclone activity sensitively. In the present model, notable tropical cyclone activity only occurs in ocean basins with a closed cyclonic streamline pattern. Consequently, there is a pouch region

(cf. Dunkerton et al., 2009) where tropical cyclogenesis favorably can take place. The circulation pattern resembles a monsoon trough as observed in the west Pacific and the cyclogenesis locations agree qualitatively with those found in this region (see Feng et al., 2014). A modification of the Walker circulation by the SST anomaly provides an explanation for the change of the circulation pattern. In the subsidence regions, the vorticity decreases by the divergence and the closed cyclonic circulation pattern vanishes. This is in accordance with the findings by Zhao and Held (2012) and shows that the dynamical impact on the flow should be considered besides the modification of thermodynamic factors by subsidence. Observations also suggest a relevance of dynamical factors. Vimont and Kossin (2007) found that the Atlantic meridional mode (AMM) is significantly correlated with tropical cyclone activity. This mode includes beside an SST anomaly a flow pattern that resembles in some aspects the zones with flow convergence seen in Figure 11 where tropical cyclones form favorably (see Kossin & Vimont, 2007, Figure SB 1). Furthermore, Merlis et al. (2013) detected a sensitive dependence of genesis locations and frequency with a poleward shift of the Intertropical Convergence Zone (ITCZ) in aquaplanet simulations for different radiative forcings. The enhancement of ambient vorticity in the ITCZ due to the shift likely explains this result.

The idealized experiments of this study confirm the nonlocality of tropical cyclones in the climate system indeed. Possible physical mechanisms for this outcome were disclosed. Nevertheless, the experiments are based on one model that only has a quite coarse resolution for tropical cyclone modeling. Wehner et al. (2015) found that the sign of tropical cyclone number change in future projections depends on the resolution. However, change pattern of their simulations coincide when the low-resolution tropical cyclones were compared with the category 4 and 5 tropical cyclones in the high resolution. Therefore, the inconsistency in the signal could stem from the fact that tropical cyclones in a low-resolution model would become more intense at a higher model resolution. This statement is also in agreement with the findings of Bengtsson et al. (2007) and Li et al. (2013) who also investigated the impact of different resolutions on tropical cyclones in their global models. Anyhow, it would be of interest to study what PlaSim at higher resolution and other models might simulate with the same experimental setup. An idealized model intercomparison study could help to gain more confidence in the mechanism and to learn why different models give different answers in realistic climate projections. Investigating the sensitivity of the model results with respect to the magnitude of the SST anomaly would also be a crucial research problem. Another interesting question is to investigate the impact of land surface properties on tropical cyclones. We found a significant sensitivity to albedo that could be influenced by vegetation. These issues could be suitable for future studies.

Acknowledgments
This work was supported through the Cluster of Excellence 'CliSAP' (EXC177), Universität Hamburg, funded through the German Science Foundation (DFG). The authors thank two anonymous reviewers for their constructive comments. The model code of PlaSim and instructions for repeating the model experiments are available at https://www.clisap.de/research/b:-climate-manifestations-and-impacts/crg-dynamical-systems/nonlocality-of-tropical-cyclone-activity/.

References

Abdullah, S. M. A. (2015). *Sensitivity of tropical cyclone activity to sea surface temperature anomalies in a global climate model* (Master thesis, 59 pp.). Hamburg, Germany: School of Integrated Climate System Science, Universität Hamburg.

Bacmeister, J. T., Reed, K. A., Hannay, C., Lawrence, P., Bates, S., Truesdale, J. E., . . . Levy, M. (2016). Projected changes in tropical cyclone activity under future warming scenarios using a high-resolution climate model. *Climatic Change*, 1–14. https://doi.org/10.1007/s10584-016-1750-x

Ballinger, A. P., Merlis, T. M., Held, I. M., & Zhao, M. (2015). The sensitivity of tropical cyclone activity to off-equatorial thermal forcing in aquaplanet simulations. *Journal of the Atmospheric Sciences*, *72*, 2286–2302. https://doi.org/10.1175/JAS-D-14-0284.1

Bell, G. D., Halpert, M. S., Schnell, R. C., Higgins, R. W., Lawrimore, J., Kousky, V. E., . . . Artusa, A. (2000). Climate assessment for 1999. *Bulletin of the American Meteorological Society*, *81*, S1–S50. https://doi.org/10.1175/1520-0477(2000)81[s1:CAF]2.0.CO;2

Bengtsson, L., Hodges, K. I., Esch, M., Keenlyside, N., Kornblueh, L., Luo, J. J., & Yamagata, T. (2007). How may tropical cyclones change in a warmer climate? *Tellus, Series A*, *59*, 539–561. https://doi.org/10.1111/j.1600-0870.2007.00251.x

Bister, M., & Emanuel, K. A. (2002). Low frequency variability of tropical cyclone potential intensity, 1, Interannual to interdecadal variability. *Journal of Geophysical Research*, *107*(D24), 4801. https://doi.org/10.1029/2001JD000776

Camargo, S. J., Tippett, M. K., Sobel, A. H., Vecchi, G. A., & Zhao, M. (2014). Testing the performance of tropical cyclone genesis indices in future climates using the HiRAM model. *Journal of Climate*, *27*, 9171–9196. https://doi.org/10.1175/JCLI-D-13-00505.1

Chiang, J. C., & Vimont, D. J. (2004). Analogous Pacific and Atlantic meridional modes of tropical atmosphere–ocean variability. *Journal of Climate*, *17*, 4143–4158. https://doi.org/10.1175/JCLI4953.1

Dunkerton, T. J., Montgomery, M. T., & Wang, Z. (2009). Tropical cyclogenesis in a tropical wave critical layer: Easterly waves. *Atmospheric Chemistry and Physics*, *9*(15), 5587–5646. https://doi.org/10.5194/acp-9-5587-2009

Emanuel, K. (2010a). Tropical cyclone activity downscaled from NOAA-CIRES reanalysis, 1908–1958. *Journal of Advances in Modeling Earth Systems*, *2*, 1. https://doi.org/10.3894/JAMES.2010.2.1

Emanuel, K. (2013). Downscaling CMIP5 climate models shows increased tropical cyclone activity over the 21st century, *Proceedings of the National Academy of Sciences of the United States of America*, *110*, 12219–12224. https://doi.org/10.1073/pnas.1301293110

Emanuel, K., & Nolan, D. (2004). Tropical cyclone activity and the global climate system. In *Preprints, 26th conference on hurricanes and tropical meteorology* (pp. 240–241). Boston, MA: American Meteorological Society.

Emanuel, K. (2010b). Stratospheric cooling and tropical cyclones. In *Preprints, 29th conference on hurricanes and tropical meteorology* (p. 4A.4). Boston, MA: American Meteorological Society.

Feng, T., Chen, G.-H., Huang, R.-H., & Shen, X.-Y. (2014). Large-scale circulation patterns favourable to tropical cyclogenesis over the western North Pacific and associated barotropic energy conversions. *International Journal of Climatology*, *34*, 216–227. https://doi.org/10.1002/joc.3680

Fraedrich, K., Jansen, H., Kirk, E., Luksch, U., & Lunkeit, F. (2005). The planet simulator: Towards a user friendly model. *Meteorologische Zeitschrift*, *14*(3), 299–304. https://doi.org/10.1127/0941-2948/2005/0043

Gray, W. M. (1979). Hurricanes: Their formation, structure and likely role in the tropical circulation. In D. B. Shaw (Ed.), *Meteorology over the tropical oceans* (pp. 155–218). Bracknell, UK: Royal Meteorological Society.

Hart, R. E. (2003). A cyclone phase space derived from thermal wind and thermal asymmetry. *Monthly Weather Review*, *131*, 585–616. https://doi.org/10.1175/1520-0493(2003)131<0585:ACPSDF>2.0.CO;2

Knutson, T. R., McBride, J. L., Chan, J., Emanuel, K., Holland, G., Landsea, C., . . . Sugi, M. (2010). Tropical cyclones and climate change. *Nature Geoscience*, *3*, 157–163. https://doi.org/10.1038/ngeo779

Kossin, J. P., & Vimont, D. J. (2007). A more general framework for understanding Atlantic hurricane variability and trends. *Bulletin of the American Meteorological Society*, *88*, 1767–1781. https://doi.org/10.1175/BAMS-88-11-1767

Kuo, H. L. (1974). Further studies of the parameterization of the influence of cumulus convection on large-scale flow. *Journal of the Atmospheric Sciences*, *31*, 1232–1240. https://doi.org/10.1175/1520-0469(1974)031<1232:FSOTPO>2.0.CO;2

Lacis, A. A., & Hansen, J. E. (1974). A parameterization for the absorption of solar radiation in the Earth's atmosphere. *Journal of the Atmospheric Sciences*, *31*, 118–133. https://doi.org/10.1175/1520-0469(1974)031<0118:APFTAO>2.0.CO;2

Li, F., Collins, W. D., Wehner, M. F., & Leung, L. R. (2013). Hurricanes in an aquaplanet world: Implications of the impacts of external forcing and model horizontal resolution. *Journal of Advances in Modeling Earth Systems*, *5*, 134–145. https://doi.org/10.1002/jame.20020

Louis, J. F. (1979). A parametric model of vertical eddy fluxes in the atmosphere. *Boundary-Layer Meteorology*, *17*, 187–202. https://doi.org/10.1007/BF00117978

Louis, J. F., Tiedtke, M., & Geleyn, M. (1982). *A short history of the PBL parameterization at ECMWF*. Paper presented at ECMWF workshop on planetary boundary layer parameterization. *Reading*, November 25–27.

Lunkeit, F., Blessing, S., Fraedrich, K., Jansen, H., Kirk, E., Luksch, U., & Sielmann, F. (2011a). *Planet simulator user's guide version 16* (technical report, 70 pp.). Hamburg, Germany: University of Hamburg. Retrieved from https://www.mi.uni-hamburg.de/en/arbeitsgruppen/theoretische-meteorologie/modelle/sources/psusersguide.pdf

Lunkeit, F., Borth, H., Böttinger, M., Fraedrich, K., Jansen, H., Kirk, E., . . . Wan, H. (2011b). *Planet simulator reference manual version 16* (technical report, 85 pp.). Hamburg, Germany: University of Hamburg. Retrieved from https://www.mi.uni-hamburg.de/en/arbeitsgruppen/theoretische-meteorologie/modelle/sources/psreferencemanual.pdf

Merlis, T. M., Zhao, M., & Held, I. M. (2013). The sensitivity of hurricane frequency to ITCZ changes and radiatively forced warming in aquaplanet simulations. *Geophysical Research Letters*, *40*, 4109–4114. https://doi.org/10.1002/grl.50680

Oouchi, K., Yoshimura, J., Yoshimura, H., Mizuta, R., Kusunoki, S., & Noda, A. (2006). Tropical cyclone climatology in a global-warming climate as simulated in a 20 km-mesh global atmospheric model: Frequency and wind intensity analyses. *Journal of the Meteorological Society of Japan*, *84*(2), 259–276. https://doi.org/10.2151/jmsj.84.259

Polvani, L. M., Scott, R. K., & Thomas, S. J. (2004). Numerically converged solutions of the global primitive equations for testing the cynamical core of atmospheric GCMs. *Monthly Weather Review*, *132*, 2539–2552. https://doi.org/10.1175/MWR2788.1

Ramsay, H. A., & Sobel, A. H. (2011). Effects of relative and absolute sea surface temperature on tropical cyclone potential intensity using a single-column model. *Journal of Climate*, *24*, 183–193. https://doi.org/10.1175/2010JCLI3690.1

Reed, K. A., & Jablonowski, C. (2011). An analytic vortex initialization technique for idealized tropical cyclone studies in AGCMs. *Monthly Weather Review*, *139*, 689–710. https://doi.org/10.1175/2010MWR3488.1

Roeckner, E., Arpe, K., Bengtsson, L., Brinkop, S., Dümenil, L., Esch, M., . . . Windelband, M. (1992). *Simulation of the present-day climate with the ECHAM-3 model: Impact of model physics and resolution* (Rep. 93, 171 pp.). Hamburg, German: Max-Planck Institut für Meteorologie.

Sasamori, T. (1968). The radiative cooling calculation for application to general circulation experiments. *Journal of Applied Meteorology and Climatology*, *7*, 721–729. https://doi.org/10.1175/1520-0450(1968)007<0721:TRCCFA>2.0.CO;2

Simpson, R. H. (1974). The hurricane disaster potential scale. *Weatherwise*, *27*(4), 169–186. https://doi.org/10.1080/00431672.1974.9931702

Sobel, A. H., Held, I. M., & Bretherton, C. S. (2002). The ENSO signal in tropical tropospheric temperature. *Journal of Climate*, *15*, 2702–2706. https://doi.org/10.1175/1520-0442(2002)015<2702:TESITT>2.0.CO;2

Stephens, G. L. (1984). The parameterization of radiation for numerical weather prediction and climate models. *Monthly Weather Review*, *112*, 826–867. https://doi.org/10.1175/1520-0493(1984)112<0826:TPORFN>2.0.CO;2

Sugi, M., Murakami, H., & Yoshimura, J. (2009). A reduction in global tropical cyclone frequency due to global warming. *SOLA*, *5*, 164–167. https://doi.org/10.2151/sola.2009-042

Swanson, K. L. (2008). Nonlocality of Atlantic tropical cyclone intensities. *Geochemistry, Geophysics, Geosystems*, *9*, Q04V01. https://doi.org/10.1029/2007GC001844

Tanaka, H. L., Ishizaki, N., & Kitoh, A. (2004). Trend and interannual variability of Walker, monsoon and Hadley circulations defined by velocity potential in the upper troposphere. *Tellus, Series A*, *56*, 250–269. https://doi.org/10.1111/j.1600-0870.2004.00049.x

Tang, B. H., & Neelin, J. D. (2004). ENSO influence on Atlantic hurricanes via tropospheric warming. *Geophysical Research Letters*, *31*, L24204. https://doi.org/10.1029/2004GL021072

Trenberth, K. E. (1997). The definition of El Niño. *Bulletin of the American Meteorological Society*, *78*, 2771–2777. https://doi.org/10.1175/1520-0477(1997)078<2771:TDOENO>2.0.CO;2

Vecchi, G. A., & Soden, B. J. (2007). Effect of remote sea surface temperature change on tropical cyclone potential intensity. *Nature*, *450*, 1066–1070. https://doi.org/10.1038/nature06423

Vecchi, G. A., Swanson, K. L., & Soden, B. J. (2008). Whither hurricane activity? *Science*, *322*(5902), 687–689. https://doi.org/10.1126/science.1164396

Vimont, D. J., & Kossin, J. P. (2007). The Atlantic Meridional Mode and hurricane activity. *Geophysical Research Letters*, *34*, L07709. https://doi.org/10.1029/2007GL029683

Wehner, M., Prabhat, Reed, K. A., Stone, D., Collins, W. D., & Bacmeister, J. (2015). Resolution dependence of future tropical cyclone projections of CAM5.1 in the U.S. CLIVAR hurricane working group idealized configurations. *Journal of Climate*, *28*, 3905–3925. https://doi.org/10.1175/JCLI-D-14-00311.1

Zhang, W., Vecchi, G. A., Villarini, G., Murakami, H., Rosati, A., Yang, X., Jia, L., & Zen, F. (2017). Modulation of western North Pacific tropical cyclone activity by the Atlantic Meridional Mode. *Climate Dynamics*, *48*(1), 631–647. https://doi.org/10.1007/s00382-016-3099-2

Zhao, M., & Held, I. M. (2012). TC-permitting GCM simulations of hurricane frequency response to sea surface temperature anomalies projected for the late-twenty-first century. *Journal of Climate*, *25*, 2995–3009. https://doi.org/10.1175/JCLI-D-11-00313.1

Zhao, M., Held, I. M., Lin, S., & Vecchi, G. A. (2009). Simulations of global hurricane climatology, interannual variability, and response to global warming using a 50-km resolution GCM. *Journal of Climate*, *22*, 6653–6678. https://doi.org/10.1175/2009JCLI3049.1